Influence of Graphite Morphology on the Fatigue Behaviour of Nodular Cast Iron

Predrag Čanžar[1,a] , Zdenko Tonković[2,b] and Janoš Kodvanj[2,c]

[1] Končar – Electrical Engineering Institute, Inc., Fallerovo šetalište 22, 10002 Zagreb, Croatia

[2] Faculty of Mechanical Engineering and Naval Architecture, University of Zagreb
I. Lučića 5, 10000 Zagreb, Croatia

[a] pcanzar@koncar-institut.hr, [b] ztonkov@fsb.hr, [c] janos.kodvanj@fsb.hr

Keywords: nodular cast iron, microstructure, fatigue, experiment, finite element method.

Abstract. Paper presents an experimental and numerical investigation of the cyclic deformation processes as well as low-cycle fatigue behaviour of the four different types of nodular cast iron EN-GJS-400-18-LT. The experimental part of this study consists of monotonic tensile tests, symmetric and unsymmetric, strain-controlled, cyclic tests, conducted on smooth cylindrical specimens, while the fatigue crack initiation and propagation, as well as fracture toughness tests are conducted on the compact tension and single edged notched specimens under various loading regimes. During the tests, monitoring of the crack length is performed by an optical system. Experimental results show that different material types have significantly different crack behaviour. Within the framework of numerical investigations an efficient algorithm for modelling of cyclic plasticity is examined. This algorithm is implemented into the finite element program ABAQUS and applied to the analysis of a crack growth near the notch. The accuracy of the computational procedure is tested by comparing the computed results with the real experimental data.

Introduction

The ductile nodular cast iron grade EN-GJS-400-18-LT, in which graphite spheroids or nodules in a ferritic matrix provide large ductility and fatigue strength, is widely used [1]. It is well-known that fatigue strength is influenced by the graphite morphology (size, shape and distribution of graphite nodules) as well as by microstructure phase (ferritic and pearlitic) [2, 3]. Aiming to prevent catastrophic failures and to prolong the service lifetime of cyclically loaded structures, it is important to consider the influence of the graphite nodule features on the fatigue crack initiation and propagation at the root of a geometrical discontinuities and local notches. As reported in [4, 5], when a fatigue crack is nucleated and propagates into the vicinity of the notch, the crack growth rate of short cracks is generally higher than that can be predicted by using the stress intensity factor concept based upon linear elastic fracture mechanics. Thus, it becomes essential to incorporate the effect of plasticity on initiation and growth behaviour of short fatigue cracks. There are only limited experimental data available on fatigue crack growth behaviour of EN-GJS-400-18-LT and still the effect of the microstructure on fracture toughness and fatigue properties of this material is not well documented [6, 7]. The present paper is concerned with the experimental investigation and numerical modelling of the low-cycle fatigue behaviour of nodular cast iron EN−GJS−400−18−LT depending on the material microstructure.

Materials and specimens

Four types of cast iron EN−GJS−400−18−LT produced by different technologies are considered. For producing nodular cast iron, one non standard technique (type 100) and three standard techniques (Flotret − type 200, Tundish − type 300, and Inmould − type 400) are used. The material

has been provided by the company MIV Varaždin, Croatia. The graphite morphology of the casting types is shown in Fig. 1. As it can be seen, material produced by the Flotret process has significantly larger nodules with low density distribution than the other three types of nodular cast iron. Besides that, Flotret material has graphite nodules with the lowest circularity (irregularly shaped nodules) and lower content of pearlitic grain. On the other hand, Tundish, and Inmould material types have smaller ferrite grains and smaller nodules, more spherical and regular in shape than those in the Flotret material type. Furthermore, non standard material type has the highest content of pearlite while its content is least in Flotret material type. All uniaxial (monotonic and cyclic) as well as fatigue tests are conducted at room temperature on a Walter Bai servohydraulic testing machine with a load capacity of ±50 kN. Fig. 2 illustrates the schematic shape and geometry of specimens used for experimental part of research. It comprises a smooth polished cylindrical specimens used for monotonic and cyclic symmetric and unsymmetric tests (Fig. 2a) as well as compact tension (CT) for fatigue crack growth tests and single edged notched (SENB) specimen for fracture toughness tests (Fig. 2b and c), all according to the standards ASTM E606 and ASTM E647 and ASTM E1820.

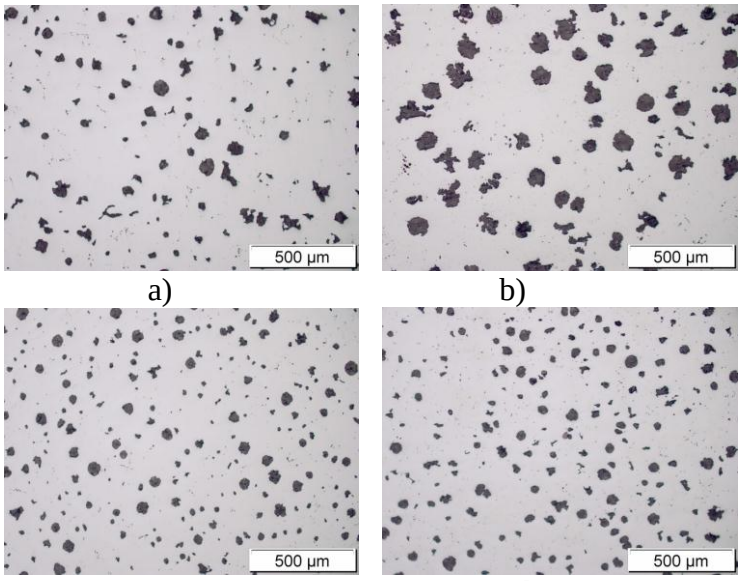

Fig. 1. Microstructure of the nodular cast iron for: a) type 100; b) type 200; c) type 300 and d) type 400

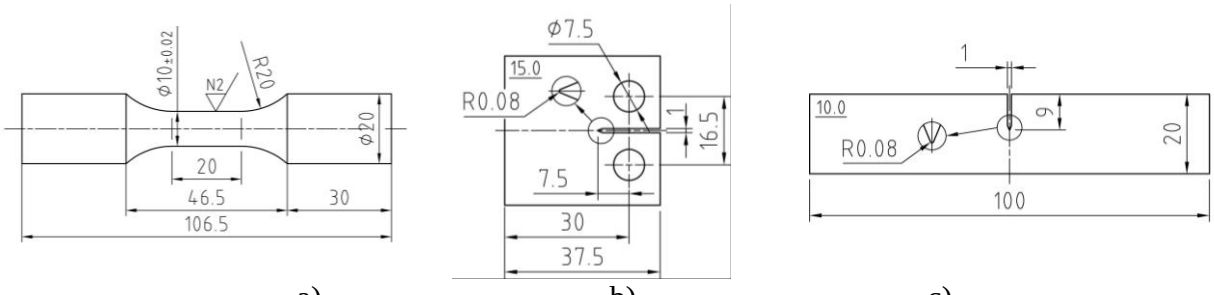

Fig. 2. Shape and dimensions of specimens: a) cylindrical specimen for monotonic and cyclic testing, b) CT specimen and c) SENB specimen

Experimental investigation

In the first part of the experimental investigation the characterization of the graphite morphology and the matrix microstructure is performed on fifty samples for every material type. It was followed by monotonic uniaxial static tests used to obtain engineering and true stress-strain curves.

Experiments are conducted using a non contact laser extensometers which allowed measurement of cross section contraction, allowing to develop a Poisson's ratio as well as true stress-strain curves. True stress-strain curves are later used to develop the Ramberg-Osgood material parameters *n* and *K*. Ramberg-Osgood's material model for describing monotonic behaviour is compared with the experimental one, and a good agreement was achieved what is shown in Fig. 3b) as well as with engineering (Fig 3a) and true stress– strain curves (Fig 3b).

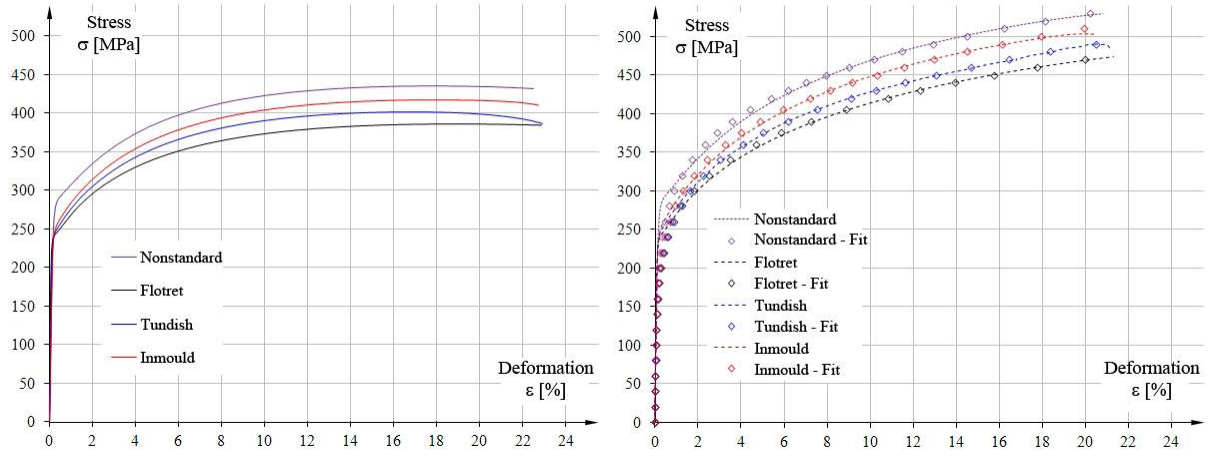

a) b)

Fig. 3. Monotonic tensile tests for four different series of nodular cast iron grade EN-GJS-400-18-LT: a) engineering stress-strain curve, b) true stress– strain curve

Mechanical properties as well as Ramberg-Osgood's material parameters of nodular cast iron grade EN-GJS-400-18-LT are systematically presented in Table 1. One can see that the Flotret series of material has the smallest and the nonstandard series has the largest value of yield and ultimate stress, while other two series of material have similar mechanical properties. In the same table, only for the comparison purposes, the critical value of *J* integral was also expressed. Considering the critical value of *J* integral, Tundish series have the largest value and consequently the strongest resistance to the crack growth. On contrary, the Flotret series have the smallest value of critical *J* integral and therefore the weakest resistance for the crack growth. The shortest specimens which standard still allows are used for uniaxial cycle tests to avoid buckling effect during compression. The strain is controlled with an extensometer of a gauge length of 10 mm (Fig. 4a).

Table 1. Mechanical properties of nodular cast iron grade EN-GJS-400-18-LT

Material Series	σ_y [MPa]	σ_u [MPa]	E [GPa]	K [MPa]	n	J_Q [kJ/m^2]
Nonstandard	286,4	435,1	163,4	700,4	0,1726	81,9
Flotret	244,0	385,8	180,0	630,4	0,1809	74,0
Tundish	250,0	402,0	215,9	666,7	0,1869	86,0
Inmould	255,8	417,2	199,9	691,3	0,1868	84,5

Cyclic tests are carried out with the constant strain rate of 10^{-3} s^{-1} limited by applied strain amplitude ($\Delta\varepsilon/2$). For symmetric cyclic test, different strain amplitude is applied from the 0.2% up to the 1.2% with the increment of 0.2%. In these tests mean strain is always equal to zero. For unsymmetrical test, mean strain and strain amplitude was kept constant (ε=0.8). In each test, 40 stress–strain hysteresis loops are obtained which is more than enough to achieve a stabilized curve, in fact stabilization of material is achieved after approximately 15 cycles, which was evident from

decreased difference between two adjoining stress ranges. Representative cyclic symmetrical ($\Delta\varepsilon/2=\pm 0.8\%$) and unsymmetrical tests are presented in Fig. 5a) and b) only for one type of material due to conciseness of this paper. More data can be found in [10]. In both tests significant cyclic hardening is observed.

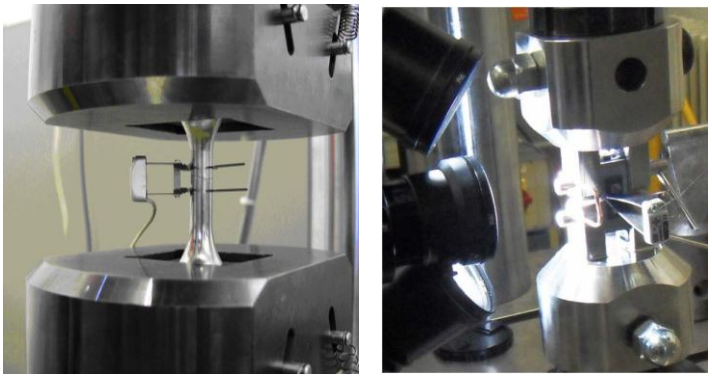

a) b)

Fig. 4. Specimen and testing configuration for: a) cylindrical specimen, b) CT specimen

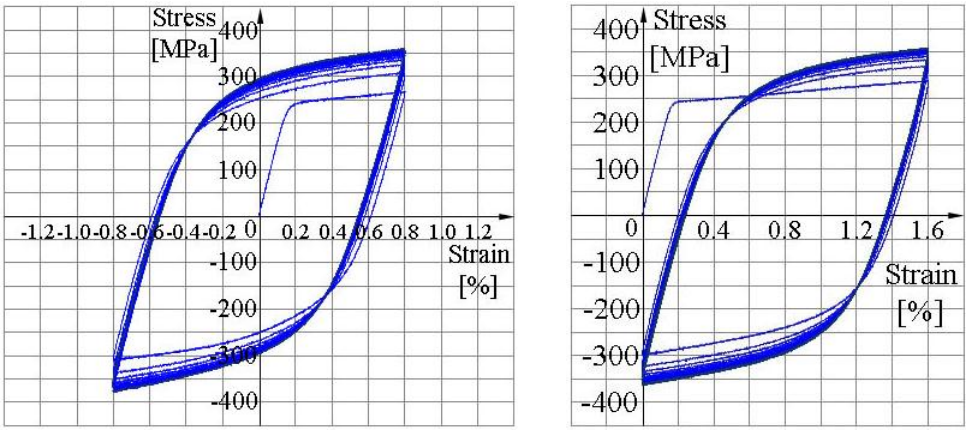

a) b)

Fig. 5. Cyclic hysteresis loops for Tundish material type: a) symmetrical and b) unsymmetrical stress–strain hysteresis loops

The hysteresis behaviour obtained in symmetrical multiple step tests is presented in Fig. 6. Therein, the strain amplitude is increased in steps of 0.2%, while keeping the mean strain equal to zero. The number of cycles at each step was 15 and the maximum strain amplitude was equal to ±1.2%. The cyclic stress-strain curve which is especially important in studies on low-cycle fatigue and crack initiation is determined by connecting the tips of the stabilized hysteresis loops obtained from specimens tested at different strain levels. The tips of the hysteresis loops are obtained with sufficient accuracy by recording a large number of experimental points. In this investigation, the least squares technique is used to determine the material properties constants, *n'* and *K'*, which describe the Ramberg-Osgood expression for the cyclic stress-strain curve. The stabilized cyclic stress-strain curve with the derived material constants for Tundish material type is shown in Fig. 6 with the bold red line. Next, the fatigue crack growth and the fracture toughness tests are performed. The monitoring of crack length during the tests is performed by an optical measuring system Aramis. The tests are conducted on the compact tension (CT) and single-edge notched

(SENB) specimens (Fig. 2b and c), loaded in three-point-bending under several *R*-ratios. Figure 7 presents the crack growth results for *R*=0.1.

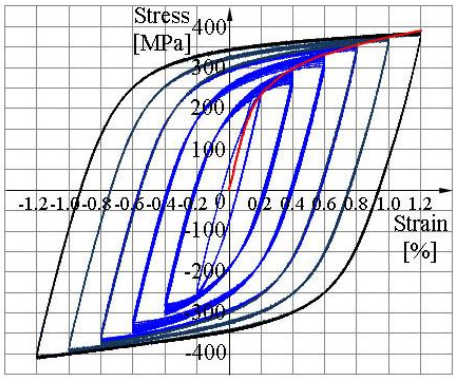

K'=900; *n*'=0.18

Fig. 6. The stabilized cyclic stress-strain curve for Tundish type of nodular cast iron

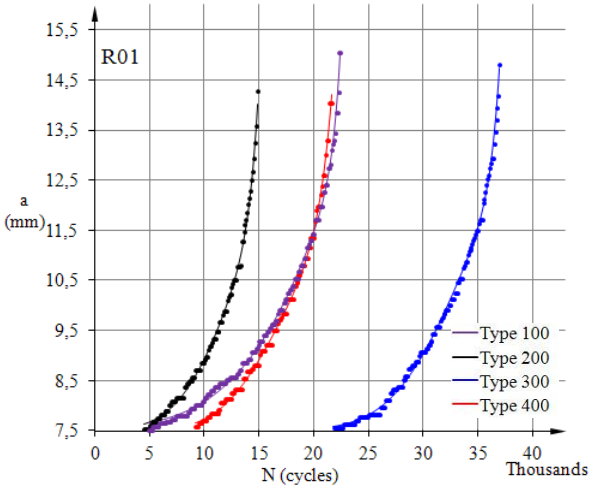

Fig. 7. Number of cycles vs. crack length for *R*=0.1

As one can see, the Tundish type of material can withstand the largest number of loading repetitions till the final fracture, while the Flotret type of material shows the least resistance for crack propagation. Since this kind of testing is long lasting, there was no reason for measuring every cycle and every small displacement of the specimen with the optical equipment. Rather than that, every 100^{th} cycle is recorded, and captured at the moment of maximum load, which is imposed by the testing machine, thanks to the 196 kHz sampling. Specimen testing and crack measurement is shown in the Fig. 4b). Besides of measuring crack propagation i.e. the crack size, crack mouth opening displacement (CMOD) is also measured using special extensometers. Due to very fast measurement, shutter time was correspondingly small, and because of that fact, lightening of the object has to be significant. It is obtained through the usage of led lighting, since it doesn't emit a large amount of heat on the nearby specimen and camera objective.

During the experiment (and thereafter) the growth of cracks can be observed and traced using one of the methods defined in the software Aramis. If cracks are expressed in the form of equivalent strains, with automatically defined limits, then the crack takes the form as shown in Fig 8. Although the crack is clearly visible, it can be more clearly shown if the boundaries of displaying equivalent strain are narrowed by a custom selected range. The pictures also show the well known crack growth path as described in detail in [11].

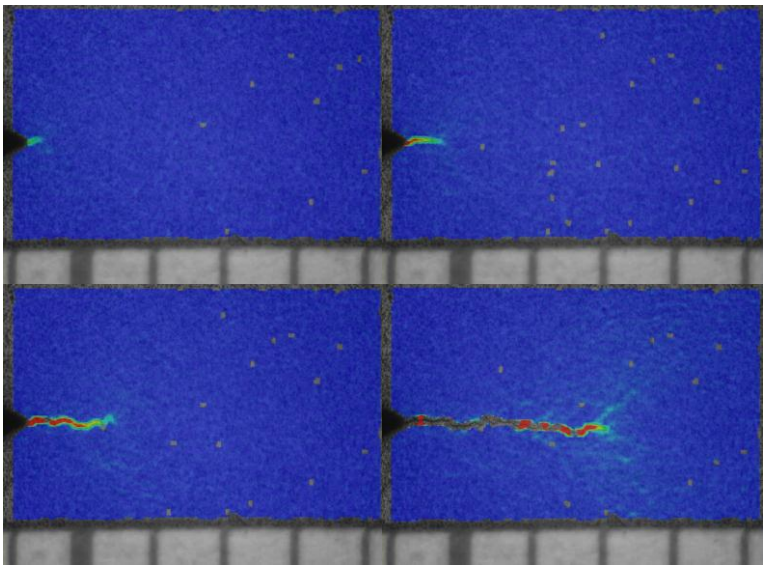

Fig. 8. Crack monitoring using the Aramis software

Numerical modelling

The accurate and realistic modelling of inelastic deformations as well as damage and failure behaviour of ductile materials under general loading conditions is still complicated problem. In this paper the algorithm which enables numerical modelling of cyclic elastoplastic deformation of shell structures proposed by Tonković et al. in 2008 is modified to simulate elastoplastic behaviour of a nodular cast iron. The derived computational algorithm is implemented in the software Abaqus/Standard [9] by using the user-defined material subroutine UMAT. More details concerning the applied computational strategy can be found in References [7, 8, 10]. Figure 9 shows a comparison of the numerical predictions and the test data obtained from the symmetric strain-controlled cyclic experiment. Herein, the results of numerical analysis are presented with green circles. Good agreement of the solutions is exhibited except for the first cycle, since the kinematic hardening component is calibrated using the stabilized stress-strain curve. All computations have been performed within the finite element software Abaqus/Standard.

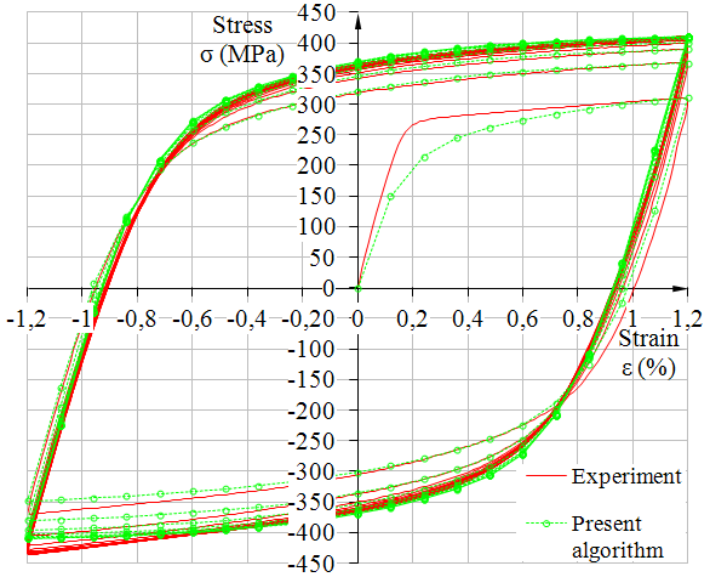

Fig. 9. Comparison of the test data and the simulated model for representative stress–strain hysteresis loops

The cyclic plasticity model is afterwards applied to study the fatigue damage near the notch and the crack tip. Thereby, Abaqus/Standard damage initiation and evolution criteria are used to determine the low-cycle fatigue damage. These two criteria are based on the stabilized accumulated inelastic hysteresis strain energy per cycle Δw. The cycle number in which damage is initiated is written in the form:

$$N_0 = c_1 \Delta w^{c_2}, \tag{1}$$

where c_1 and c_2 are material constants. Once the damage criterion is satisfied at the material integration point, rate of damage per cycle is given by:

$$\frac{\mathrm{d}D}{\mathrm{d}N} = \frac{c_3 \Delta w^{c_4}}{L}, \tag{2}$$

where c_3 and c_4 are material constants, L is the characteristic length associated with an integration point, while D stands for fatigue scalar damage variable which assumes the degradation of the elastic stiffness. For the cast iron Type 300 specimen, the cyclic plasticity and low-cycle fatigue material constants are as follows: $A_1 = 59.93\,\mathrm{GPa}$, $A_2 = 139.7\,\mathrm{GPa}$, $B_1 = 1.57\,\mathrm{GPa}$, $B_2 = 1.56\,\mathrm{GPa}$, $C_1 = 18.7\,\mathrm{MPa}$, $D_1 = 84.7\,\mathrm{MPa}$, $c_1 = 40067$, $c_2 = -0.26$, $c_3 = 6\mathrm{e}-5$, $c_4 = 1.5$. In order to verify the computational strategy, the fatigue damage in the CT and SENB type specimens is studied. For the CT model discretization, a plane stress quadratic element (CPS4) is applied. A typical finite element mesh applied in the analysis is shown in Figure 10a. The deformed CT specimen with opened crack is depicted in Fig. 10b. Fig. 11 shows a comparison between the experimental data and numerical predictions. As may be observed from figure, an excellent agreement of the solutions is exhibited.

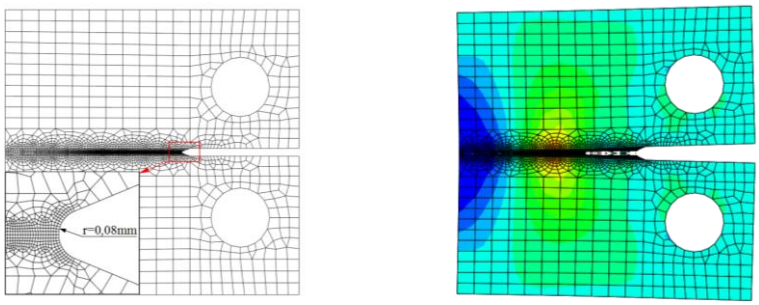

a) b)

Fig. 10. Fatigue damage analysis in the CT specimen: a) finite element mesh, b) deformed specimen

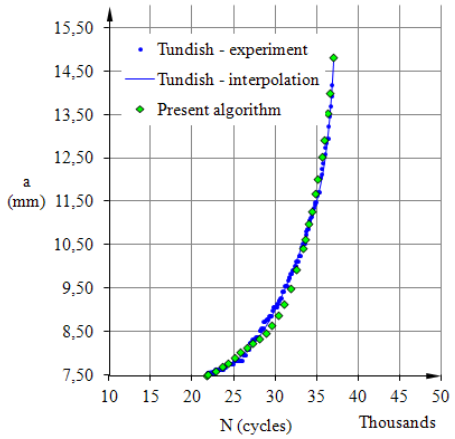

Fig. 11. Comparison between the experimental data and numerical predictions for R=0.1

Conclusion

Experimental results show that size, shape and distribution of the graphite nodules has no significant influence on cyclic hardening of the material but they play a great role in the crack initiation and propagation process. It is shown that the larger irregularly shaped nodules reduce fracture toughness and fatigue strength. Furthermore, the results demonstrated that pearlitic phase does not strongly affect fatigue life if it's share does not exceeds 10%. A computational algorithm for the integration of the cyclic plasticity constitutive model is derived and implemented in an Abaqus UMAT subroutine. The accuracy of the computational procedure for crack initiation and propagation modelling is verified by comparing the model predictions with the experimental data. It is shown that the numerical results agree well with the experimental results.

References

[1] P. Hübner, H. Schlosser, G. Pusch and H. Biermann: Load history effects in ductile cast iron for wind turbine components. International Journal of Fatigue Vol. 29 (2007), p. 1788–1796.

[2] N. Costa, N. Machado and F.S. Silva, A new method for prediction of nodular cast iron fatigue limit, International Journal of Fatigue, 32, 988–995, 2010.

[3] F. Iacoviello, O. Di Bartolomeo, V. Di Cocco and V. Piacente, Damaging micromechanisms in ferritic–pearlitic ductile cast irons, Materials Science and Engineering, A 478, 181–186, 2008.

[4] F. Ding, M. Feng and Y. Jiang., Modeling of fatigue crack growth from a notch, Int. Journal of Plasticity, 23, 1167–1188, 2007.

[5] F. Fan, S. Kalnaus and Y. Jiang, Modeling of fatigue crack growth of stainless steel 304L, Mechanics of Materials, 40 (11), 961-973, 2008.

[6] T. Mottitschka, G. Pusch, H. Biermann, L. Zybell and M. Kuna: Influence of overloads on the fatigue crack growth in nodular cast iron experiments and numerical simulation. Procedia Engineering Vol. 2 (2010), p. 1557-1567.

[7] P. Čanžar, Z. Tonković, A. Bakić and J. Kodvanj: Experimental and Numerical Investigation of Fatigue Behaviour of Nodular Cast Iron. Key Engineering Materials Vol. 488-489 (2011), p. 182-185.

[8] Z. Tonković, J. Sorić and I. Skozrit: On numerical modeling of cyclic elastoplastic response of shell structures. Computer Modeling in Engineering & Sciences (CMES) Vol. 26 (2) (2008), 75-90.

[9] Abaqus/Standard 6.10.1, Dassault Systemes, Simulia.

[10] P. Čanžar: Experimental and Numerical Modelling of Fatigue Behaviour of Nodular Cast Iron, Doctoral Thesis, University Of Zagreb, Croatia, Faculty Of Mechanical Engineering And Naval Architecture, Zagreb, 2012.

[11] T. L. Anderson, Fracture Mechanics: Fundamentals and Applications. Structural Reliability Technology, CRC Press, Boulder, Colorado, USA, 2005.